

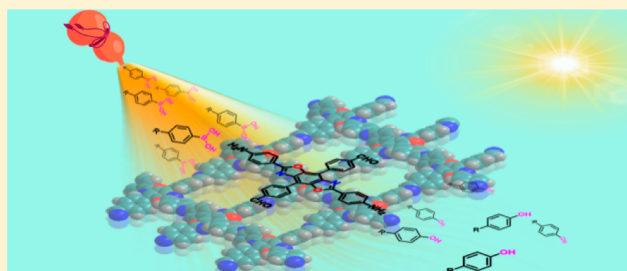
Ultrastable Covalent Organic Frameworks via Self-Polycondensation of an A₂B₂ Monomer for Heterogeneous Photocatalysis

Xiaoli Yan, Huan Liu, Yusen Li, Weiben Chen, Ting Zhang, Ziqiang Zhao, Guolong Xing, and Long Chen*[✉]

Department of Chemistry and Tianjin Key Laboratory of Molecular Optoelectronic Science, Tianjin University, Tianjin 300072, China

Supporting Information

ABSTRACT: Easy preparation, high stability, prominent activity, and excellent recyclability are four key elements for high-performance heterogeneous photocatalysts. Developing covalent organic framework (COF)-based heterogeneous photocatalysts possessing all of these traits is highly challenging. In this study, we successfully synthesized an imine-linked BBO-COF by the “two-in-one” strategy featuring the above four merits. Highly crystalline and porous BBO-COF can be easily prepared in at least 11 different simplex solvents independent of their polarity and boiling points and even under an air atmosphere. Moreover, BBO-COF exhibits extraordinary chemical stability and photostability in strong acid (12 M HCl), corrosive base (12 M NaOH), and visible light for 7 days. Furthermore, BBO-COF exhibited prominent photocatalytic activity toward oxidative hydroxylation reaction of arylboronic acids with excellent substrates tolerance and reusability. This “two-in-one” design strategy open a new avenue for facile constructing novel functional COFs with tailor-made properties.



INTRODUCTION

Covalent organic frameworks (COFs) are a novel class of porous and crystalline polymers connected by strong covalent bonds.^{1–6} Because of their large porosity, predesigned structure, tunable chemical composition, and tailor-made properties, COFs are explored as functional materials in various fields, such as gas sorption and separation,^{7–11} heterogeneous catalysis,^{12–19} energy storage,^{20–24} sensing,^{25–31} drug delivery,^{32–35} optoelectronics,^{36–42} and so on. Among them, photocatalytic COFs have recently attracted increasing attention, since their extended π -conjugated frameworks are beneficial for absorbing light, the large porosity and open channels are conducive to exposing more active sites, and the insoluble characteristics facilitate catalysts recycling.^{43–46} However, most COFs are photounstable upon light irradiation during the photocatalysis, which limits their practical applications. Thus, great efforts have been devoted to improve the stability, especially the photostability of COFs. Up to now, several strategies including utilizing the reversible/irreversible cascade reactions have been applied to prepare both chemically stable and photostable COFs.^{46,52} However, because the majority of COFs are synthesized via the co-condensation of two or more monomers,^{47–50} they suffer from the time-consuming screening process of specific synthetic conditions including solvent combinations, reaction temperature, vacuum/inert atmosphere, and so on to achieve high crystallinity.^{51,52} Thus, it is of great significance to explore a new strategy for easy preparation of COFs with high stability, excellent catalytic performance, and easy recyclability simulta-

neously for photocatalysis. Recently, our group developed a new approach based on self-condensation of bifunctional monomers (i.e., “two-in-one” strategy) for COFs synthesis.⁵³ The stoichiometry of the functional groups for condensation was kept identically equal in either homogeneous or heterogeneous conditions over various solvent systems guaranteed by this strategy. Therefore, the synthesis of COFs was simplified with better solvent adaptability and improved crystallinity as well as reproducibility.

Herein, we designed and synthesized a new bifunctional monomer 4,4'-(2,6-bis(4-aminophenyl)benzo[1,2-*d*:4,5-*d'*]bis(oxazole)-4,8-diyl)dibenzaldehyde (Figure 1a, BBO) with two formyl and two amino groups in a single benzoxazole core which was further applied to construct benzoxazole-based imine COF (BBO-COF) through intermolecular self-condensation. Unlike most reported COFs prepared by the co-condensation method which are synthesized upon tedious solvent combinations screening process to achieve high crystallinity,⁵⁴ the bifunctional monomer (BBO) can be used to prepare BBO-COF with good crystallinity in more than 11 different simplex organic solvent systems (e.g., *n*-butanol (*n*-BuOH), ethanol, methanol, mesitylene, tetrahydrofuran (THF), acetone, *N,N*-dimethylacetamide (DMAC), dichloromethane (DCM), benzyl alcohol, dioxane, *o*-dichlorobenzene (*o*-DCB), etc.) and even under air. Moreover, BBO-COF

Received: July 31, 2019

Revised: September 30, 2019

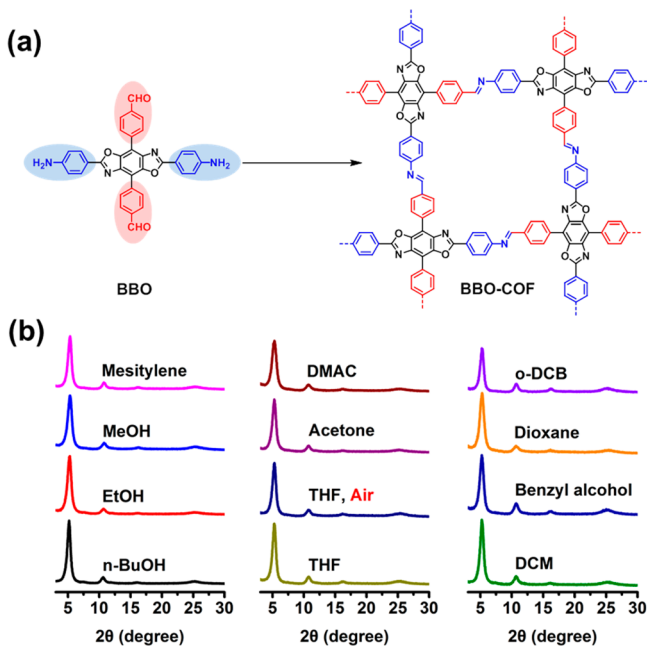


Figure 1. (a) Schematic illustration of the molecular design and synthesis of BBO-COF. (b) PXRD patterns of BBO-COFs prepared under different conditions.

exhibits extraordinary stability in strong acid (12 M HCl), corrosive base (12 M NaOH), and visible light irradiation for at least 7 days. Furthermore, BBO-COF was verified to exhibit excellent photocatalytic performances on aerobic oxidative hydroxylation of arylboronic acids with retained crystallinity after 10 runs of recycling catalysis.

RESULTS AND DISCUSSION

Synthesis and Structural Characterization. As shown in Scheme S1, BBO was synthesized in high yield and unambiguously characterized by NMR and MALDI-TOF MS (Figures S2–S4). In a typical synthetic procedure of BBO-COFs (Scheme S2), BBO (28 mg, 0.05 mmol) was suspended in a simplex organic solvent (1 mL) and 6 M acetic acid (0.1 mL) followed by refluxing for 72 h to afford brownish-yellow crystalline solids (denoted as BBO-COF_{solvent}) in high yields of 90–95%. The as-synthesized BBO-COFs were characterized by various techniques (Supporting Information). As shown in Figure S6, the FT-IR spectra of BBO-COFs prepared in different solvents were nearly identical. For example, the stretching bands of free amine (N–H, $\sim 3300\text{ cm}^{-1}$) and formyl groups (C=O, 1684 cm^{-1}) disappeared, and a new C=N stretching vibration band appeared at 1549 cm^{-1} , confirming the new generation of imine bonds in BBO-COFs.⁵⁵ Solid-state ^{13}C cross-polarization/magic angle spinning nuclear magnetic resonance (CP/MAS NMR) spectroscopy further revealed the existence of imine linkages, which exhibited an intensive characteristic peak at 153 ppm (Figure S5).⁵⁵

The crystalline structures of BBO-COFs prepared under different conditions were confirmed by powder X-ray diffraction (PXRD) analysis. As presented in Figure 1b, the powder samples obtained in all these 11 solvents exhibited same patterns, indicating identical structures, facile preparation, and good reproducibility of BBO-COFs prepared in different solvents. For convenience, BBO-COF_{BuOH} prepared in *n*-BuOH was selected as the representative for further detailed analysis. The computational structural simulations of BBO-COF_{BuOH} and Pawley refinement of PXRD were conducted by Materials Studio software. Both eclipsed stacking (AA) and staggered stacking (AB) models were considered (Figure 2). BBO-COF_{BuOH} exhibited an intense peak at 5.35°

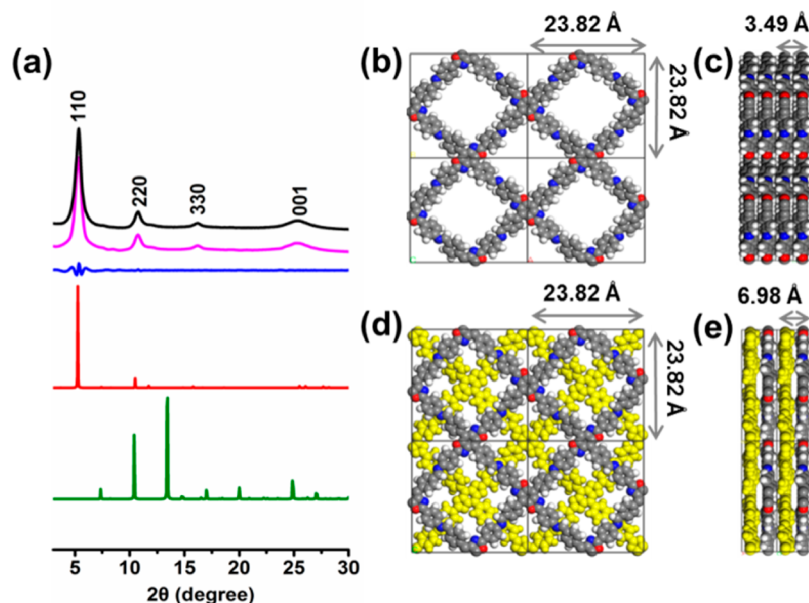


Figure 2. (a) Experimentally observed PXRD pattern of BBO-COF prepared in *n*-BuOH (black), Pawley-refined pattern (magenta), difference between the experimental and calculated data (blue), and calculated patterns for AA (red) and AB (green) stacking. (b) Top and (c) side views of the space-filling AA eclipsed stacking models of BBO-COF and the unit cells. (d) Top and (e) side views of the space-filling AB eclipsed stacking models of BBO-COF and the unit cells.

and three distinct diffractions at 10.75°, 16.20°, and 25.35°, which correspond to the 110, 220, 330, and 001 facets, respectively. The simulated PXRD patterns of the eclipsed AA stacking were in better agreement with the experimental ones compared to those of the staggered AB stacking (Figure 2a). Furthermore, the space group of BBO-COF_{BuOH} was determined to be *P*4, and the Pawley refinement afforded cell parameters of *a* = *b* = 23.82 Å, *c* = 3.49 Å, and $\alpha = \beta = \gamma = 90^\circ$ with $R_{wp} = 4.33\%$ and $R_p = 3.08\%$. Scanning electron microscopy (SEM) images disclosed that the BBO-COF_{BuOH} exhibited uniform “coral cluster”-like morphology (Figure S9a,b). Transmission electron microscopy (TEM) images revealed clear lattice stripes corresponding to the ordered nanochannel, which further confirmed the high crystallinity of the BBO-COF_{BuOH} (Figure S9c,d).

Nitrogen sorption experiments at 77 K were performed to evaluate and compare the porosities of BBO-COFs prepared under different conditions (e.g., *n*-BuOH, THF, THF under air atmosphere, *o*-DCB). All these BBO-COFs displayed type I reversible isotherms, which are characteristics of microporous structures (Figure S7a). Surprisingly, the BET surface areas for BBO-COFs prepared using different conditions were nearly the same (ca. 1070–1170 m² g⁻¹, Figure S8). The pore size distribution calculated by the nonlocal density functional (NLDFT) method of these BBO-COFs suggested a narrow pore size distribution at 1.58 nm (Figure S7b), which is in good agreement with the value of *d*-spacing observed in PXRD analysis at $2\theta = 5.35^\circ$ (1.68 nm).

Thermal Stability and Chemical Stability. To our surprise, BBO-COF exhibited extraordinarily high stability. Thermogravimetric analysis (TGA) suggested that BBO-COF retained 95% of its initial mass at 560 °C (Figure S11), and the long-range ordered framework structure could be maintained at least 400 °C (Figure S12). In addition, the BBO-COF showed excellent chemical stability. For example, the crystallinity and porosity of BBO-COF still remained after treatments of boiling water, TFA, 12 M HCl, and 12 M NaOH for 7 days. More interestingly, unlike most reported imine-linked COFs which are decomposed upon long-term light irradiation,⁴⁶ BBO-COF displayed a good tolerance to visible light irradiation. The porosity as well as the crystallinity was retained after irradiating with an 18 W white-light-emitting diodes (LED) for 7 days (Figures 3, Figures S13 and S14). The high chemical stability and photostability render BBO-COF as a good candidate for heterogeneous photocatalysis.

Heterogeneous Photocatalysis on Oxidative Hydroxylation of Arylboronic Acids. Phenols are well-known and important intermediates for natural products, polymers, and pharmaceutical medicines.^{56–58} Photocatalytic oxidative hydroxylation of arylboronic acids is an effective way to prepare the corresponding phenols.^{46,59–62} Prior to our work, several porous polymers containing a benzoxazole core have already shown photocatalytic activities toward the oxidative hydroxylation of arylboronic acids.⁴⁶ Thus, the transformation of 4-formylphenylboronic acid (1a) to 4-formylphenol (2a) was first chosen to evaluate the photocatalytic performance of BBO-COF. The photocatalysis factors including the photocatalyst, sacrificial agents, light source, and oxygen source that may influence this transformation were systematically assessed (Figure 4). As shown in Figure 4b, the reaction occurred smoothly to afford the desired 4-formylphenol (2a) in 99% yield after 48 h with BBO-COF as the photocatalyst and *N,N*-diisopropylethylamine (DIPEA) as the sacrificial electron

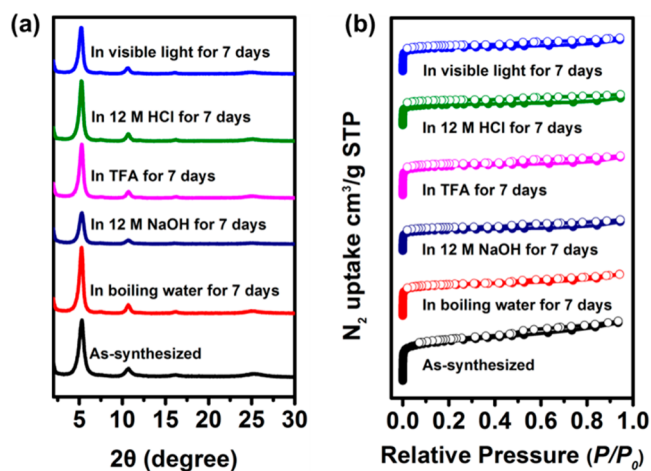


Figure 3. (a) PXRD profiles of BBO-COFs before (black) and after treatments in visible light (blue), 12 M HCl (olive), TFA (magenta), 12 M NaOH (navy), and boiling water (red) for 7 days. (b) N₂ sorption isotherms of BBO-COFs before (black) and after treatments in visible light (blue), 12 M HCl (olive), TFA (magenta), 12 M NaOH (navy), and boiling water (red) for 7 days.

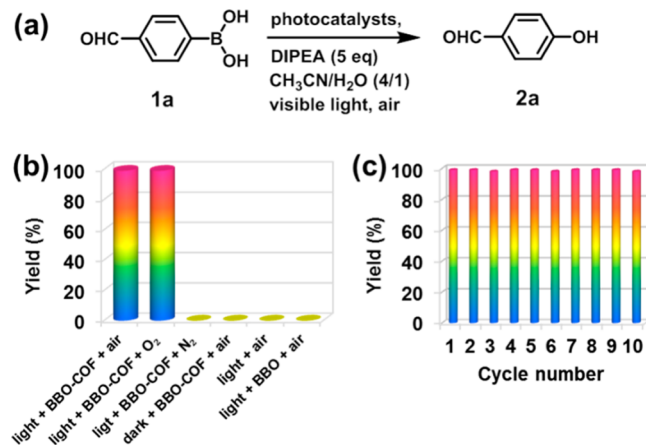


Figure 4. Photocatalytic oxidative hydroxylation. (a) Photocatalytic reaction for oxidative hydroxylation of 4-formylphenylboronic acid. (b) Control experiments for oxidative hydroxylation of 4-formylphenylboronic acid under different conditions. (c) Assessment of the reusability of BBO-COF on the oxidative hydroxylation of 4-formylphenylboronic acid.

donor under oxygen or air atmosphere. In sharp contrast, no reaction took place in the absence of BBO-COF, which indicated that BBO-COF plays a critical role as photocatalyst in this chemical transformation. Similarly, when the reaction was conducted under a dark or N₂ atmosphere, this transformation was also hard to realize. In addition, no target product was formed when BBO monomer was used instead of BBO-COF, which is basically consistent with the literature reports.⁴⁶ Therefore, it can be concluded that the photocatalytic properties of BBO-COF are not only derived from the benzoxazole moiety but also related to the π -conjugated crystalline framework. All these control experiments validated the essential roles of the photocatalyst, visible light irradiation, and oxygen in this reaction. Furthermore, to give more insights into the kinetics, the time-dependent conversions were monitored by NMR analysis. As shown in Figures S20 and S21 as well as Table S1, the conversions of 4-hydroxy-

benzaldehyde gradually increased with reaction time and reached a full conversion after nearly 48 h.

Given the insolubility of BBO-COF in common organic solvents, it can be easily separated from the reaction mixture by centrifugation. Thus, the recyclability of BBO-COF as photocatalyst was evaluated by the cycling experiments on oxidative hydroxylation of 4-formylphenylboronic acid. As shown in Figure 4c, after ten cycles, the conversion efficiency of 4-formylphenylboronic acid to 4-formylphenol still reach up to 99% with BBO-COF as the photocatalyst. Notably, the crystallinity and porosity of BBO-COF after 10 runs of cyclic reactions are still maintained and comparable with that of the pristine samples only with slight decrease⁴⁶ on PXRD peak intensity and BET surface area (Figures S16–S19).

To verify the adaptability of BBO-COFs as photocatalysts toward the conversion of arylboronic acids to the corresponding phenols, a series of arylboronic acid derivatives were tested (Table 1). As shown in Table 1, all the substrates can be

Table 1. Substrate Tolerance Tests of BBO-COF toward Oxidative Hydroxylation Reaction of Arylboronic Acids^a

$\text{Ar-B(OH)}_2 \xrightarrow[\text{CH}_3\text{CN}/\text{H}_2\text{O}(4/1), \text{visible light, air}]{\text{BBO-COF, DIPEA (5 eq)}} \text{Ar-OH}$			
entry	Ar	time (h)	yield ^b (%)
1	1-pyrenyl	96	49
2	4-MeOC ₆ H ₄	96	56
3	2-naphthyl	96	71
4	C ₆ H ₅	96	99
5	4-BrC ₆ H ₄	48	99
6	4-CHOC ₆ H ₄	48	99
7	4-NO ₂ C ₆ H ₄	48	99
8	4-CNC ₆ H ₄	30	99
9	4-MeO ₂ CC ₆ H ₄	28	99
10	4-HO ₂ CC ₆ H ₄	28	99

^aConditions: arylboronic acid (0.2 mmol), BBO-COF (21.2 mg, 0.010 mmol), CH₃CN (1.6 mL), H₂O (0.4 mL), DIPEA (1.0 mmol), irradiation with an 18 W white LED. ^bIsolated yields.

smoothly converted to the corresponding phenols with BBO-COF as photocatalyst. Generally, the reaction rates are faster for the arylboronic acids with electron-withdrawing substituents (entries 6–10) than that of arylboronic acids bearing electron-donating groups (entries 1–3). According to the reported reaction mechanism, this phenomenon could be reasonably explained by the fact that the O₂^{•-} radical anion is more accessible to the vacant p-orbital of boron atoms in arylboronic acids with electron-deficient substituents.⁵⁹

Photocatalytic Mechanism. To gain more insight into the photocatalysis process, the essential roles of the components used in the oxidative hydroxylation reaction of arylboronic acids were further investigated by a number of comparative experiments. In the absence of sacrificial agents (DIPEA), phenylboronic acid is hardly converted to the corresponding phenol with BBO-COF as the photocatalyst. Therefore, the sacrificial agent (DIPEA) is indispensable for the photocatalytic process. In addition, as discussed above, the benzoxazole-based (BBO) monomer itself exhibited no photocatalytic activity (Figure 4b). All these results motivate us to explore the reaction mechanism of the photocatalytic

process in detail. First, the UV/vis absorption spectra of BBO-COF and BBO were compared (Figure 5a and Figure S10a).

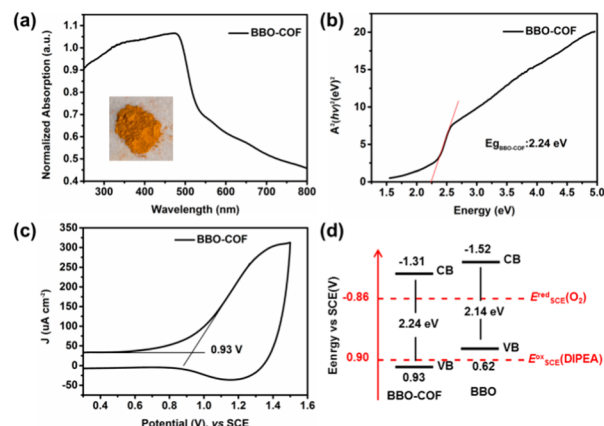


Figure 5. (a) Absorbance spectrum of BBO-COF (inset: photograph of BBO-COF). (b) Plot of Kubelka–Munk function to determine the band gap of BBO-COF. (c) Cyclic voltammogram of BBO-COF electrode in nonaqueous electrolyte. (d) Calculated alignment between the valence band and the conduction band of BBO-COF, BBO, the oxidation potential of DIPEA, and the reduction potential of O₂.

Both BBO monomer and BBO-COF showed broad absorption in the region from UV to visible light. According to the Tauc plot analysis, the optical band gaps (E_g) of BBO-COF (Figure 5b) and BBO (Figure S10b) were estimated to be 2.24 and 2.14 eV, respectively. Cyclic voltammetry (CV) was further measured to figure out the oxidation potentials of BBO-COF and BBO. The CV of both BBO-COF and BBO showed an oxidative peak with an onset at +0.93 V (Figure 5c) and +0.62 V versus the saturated calomel electrode (SCE) (Figure S8c) corresponding to the valence band (VB) potentials (E_{VB}) of 0.93 and 0.62 V, respectively. According to the optical band gaps (E_g), the approximate conduction band (CB) potentials (E_{CB}) can be calculated by the following equation:

$$E_{CB} = E_{VB} - E_g \quad (1)$$

Thus, the E_{CB} values of BBO-COF and BBO were estimated to be −1.31 and −1.52 V versus SCE, respectively. Because the oxidation potential (E^{ox}) of DIPEA is +0.90 V and the reduction potential (E^{red}) of O₂ is −0.86 V (versus SCE), the photocatalysts with E_{VB} higher than +0.90 V and E_{CB} lower than −0.86 V are capable to oxidize DIPEA, which leads to the subsequent reduction of molecular O₂.⁵⁹ It is obvious that the E_{VB} and E_{CB} of BBO-COF fully meet the above criteria while the E_{VB} of BBO is less than that of DIPEA (Figure 5d). Therefore, it is reasonable that the BBO-COF features prominent photocatalytic performance, while BBO exhibits no photocatalytic activity even with similar optical band gap. In addition, the generation of O₂^{•-} in the aid of BBO-COF was verified by electron paramagnetic resonance (EPR) spectroscopy upon adding the superoxide radical scavengers 5,5-dimethyl-1-pyrroline N-oxide (DMPO) (Figure S15). Based on the above experiments as well as the literature reports,^{59–62} a probable photocatalytic mechanism was proposed (Figure 6). The excited intermediate BBO-COF* was first generated upon visible light irradiation, and then an electron was extracted from the sacrificial electron donor (DIPEA) via a single-electron transfer (SET) process to afford the radical

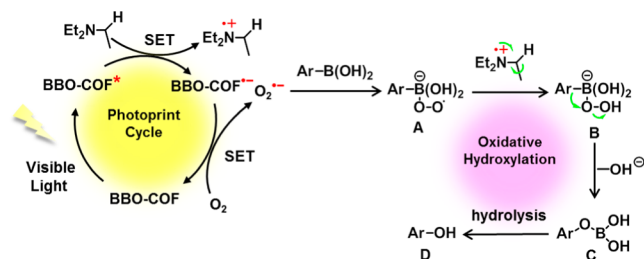


Figure 6. Probable reaction mechanism for the photocatalytic oxidative hydroxylation of arylboronic acids using BBO-COF as the photocatalyst (SET: single-electron transfer).

anion BBO-COF^{•-} together with radical cation DIPEA^{•+}. After that, BBO-COF^{•-} was oxidized by O₂ to regenerate BBO-COF for the next catalytic cycle. Meanwhile, the superoxide radical anion O₂^{•-} was formed which further added to the empty p-orbital of boron in phenylboronic acid to generate intermediate A. Intermediate A further extracted a hydrogen atom from DIPEA^{•+} to give intermediate B. After that, intermediate B is rearranged with the loss of a -OH⁻ ion to form C. The intermediate C is subsequently hydrolyzed to afford the final phenol product D.^{61,62}

CONCLUSIONS

In summary, we successfully synthesized a new photocatalytic imine-linked BBO-COF featured with four merits together of easy preparation, high stability, prominent activity, and excellent recyclability by the “two-in-one” strategy. The COF prepared by this strategy shows high crystallinity that is not affected by the solvents, which might be ascribed to the stoichiometry of the functional groups for condensation was guaranteed identically equal either in homogeneous or heterogeneous conditions over various solvent systems. The key design is to merge two formyl and two amino groups in a single benzoxazole core to form the bifunctional monomer which was further applied to construct benzoxazole-based imine COF through intermolecular self-condensation. Because of the high VB potential and low CB potential, the BBO-COF features effective catalytic activity for oxidative hydroxylation of arylboronic acids. In view of the easy preparation and good reproducibility of high quality COFs, we envision that this “two-in-one” strategy may push COF synthesis forward for practical applications.

ASSOCIATED CONTENT

Supporting Information

The Supporting Information is available free of charge on the ACS Publications website at DOI: 10.1021/acs.macromol.9b01600.

Experimental details and characterization of the monomer and BBO-COF (PDF)

AUTHOR INFORMATION

Corresponding Author

*E-mail: long.chen@tju.edu.cn (L.C.).

ORCID

Long Chen: 0000-0001-5908-266X

Notes

The authors declare no competing financial interest.

ACKNOWLEDGMENTS

This work was financially supported by National Key Research and Development Program of China (2017YFA0207500), National Natural Science Foundation of China (51973153), and the Natural Science Foundation of Tianjin City (17JCJC44600).

REFERENCES

- Côté, A. P.; Benin, A. I.; Ockwig, N. W.; O’Keeffe, M.; Matzger, A. J.; Yaghi, O. M. Porous, Crystalline, Covalent Organic Frameworks. *Science* **2005**, *310*, 1166–1170.
- Diercks, C. S.; Yaghi, O. M. The Atom, the Molecule, and the Covalent Organic Framework. *Science* **2017**, *355*, No. eaal1585.
- Ding, S.-Y.; Wang, W. Covalent Organic Frameworks (COFs): from Design to Applications. *Chem. Soc. Rev.* **2013**, *42*, 548–568.
- Feng, X.; Ding, X.; Jiang, D. Covalent Organic Frameworks. *Chem. Soc. Rev.* **2012**, *41*, 6010–6022.
- Huang, N.; Wang, P.; Jiang, D. Covalent Organic Frameworks: A Materials Platform for Structural and Functional Designs. *Nat. Rev. Mater.* **2016**, *1*, 16068.
- Wang, H.; Zeng, Z.; Xu, P.; Li, L.; Zeng, G.; Xiao, R.; Tang, Z.; Huang, D.; Tang, L.; Lai, C.; Jiang, D.; Liu, Y.; Yi, H.; Qin, L.; Ye, S.; Ren, X.; Tang, W. Recent Progress in Covalent Organic Framework Thin Films: Fabrications, Applications and Perspectives. *Chem. Soc. Rev.* **2019**, *48*, 488–516.
- Doonan, C. J.; Tranchemontagne, D. J.; Glover, T. G.; Hunt, J. R.; Yaghi, O. M. Exceptional Ammonia Uptake by a Covalent Organic Framework. *Nat. Chem.* **2010**, *2*, 235–238.
- Fan, H.; Mundstock, A.; Feldhoff, A.; Knebel, A.; Gu, J.; Meng, H.; Caro, J. Covalent Organic Framework–Covalent Organic Framework Bilayer Membranes for Highly Selective Gas Separation. *J. Am. Chem. Soc.* **2018**, *140*, 10094–10098.
- Furukawa, H.; Yaghi, O. M. Storage of Hydrogen, Methane, and Carbon Dioxide in Highly Porous Covalent Organic Frameworks for Clean Energy Applications. *J. Am. Chem. Soc.* **2009**, *131*, 8875–8883.
- Huang, N.; Krishna, R.; Jiang, D. Tailor-Made Pore Surface Engineering in Covalent Organic Frameworks: Systematic Functionalization for Performance Screening. *J. Am. Chem. Soc.* **2015**, *137*, 7079–7082.
- Zeng, Y.; Zou, R.; Zhao, Y. Covalent Organic Frameworks for CO₂ Capture. *Adv. Mater.* **2016**, *28*, 2855–2873.
- Ding, S.-Y.; Gao, J.; Wang, Q.; Zhang, Y.; Song, W.-G.; Su, C.-Y.; Wang, W. Construction of Covalent Organic Framework for Catalysis: Pd/COF-LZU1 in Suzuki–Miyaura Coupling Reaction. *J. Am. Chem. Soc.* **2011**, *133*, 19816–19822.
- Fang, Q.; Gu, S.; Zheng, J.; Zhuang, Z.; Qiu, S.; Yan, Y. 3D Microporous Base-Functionalized Covalent Organic Frameworks for Size-Selective Catalysis. *Angew. Chem., Int. Ed.* **2014**, *53*, 2878–2882.
- Han, X.; Xia, Q.; Huang, J.; Liu, Y.; Tan, C.; Cui, Y. Chiral Covalent Organic Frameworks with High Chemical Stability for Heterogeneous Asymmetric Catalysis. *J. Am. Chem. Soc.* **2017**, *139*, 8693–8697.
- Li, H.; Pan, Q.; Ma, Y.; Guan, X.; Xue, M.; Fang, Q.; Yan, Y.; Valtchev, V.; Qiu, S. Three-Dimensional Covalent Organic Frameworks with Dual Linkages for Bifunctional Cascade Catalysis. *J. Am. Chem. Soc.* **2016**, *138*, 14783–14788.
- Lu, S.; Hu, Y.; Wan, S.; McCaffrey, R.; Jin, Y.; Gu, H.; Zhang, W. Synthesis of Ultrafine and Highly Dispersed Metal Nanoparticles Confined in a Thioether-Containing Covalent Organic Framework and Their Catalytic Applications. *J. Am. Chem. Soc.* **2017**, *139*, 17082–17088.
- Yan, S.; Guan, X.; Li, H.; Li, D.; Xue, M.; Yan, Y.; Valtchev, V.; Qiu, S.; Fang, Q. Three-dimensional Salphen-Based Covalent–Organic Frameworks as Catalytic Antioxidants. *J. Am. Chem. Soc.* **2019**, *141*, 2920–2924.
- Yang, S.; Hu, W.; Zhang, X.; He, P.; Pattengale, B.; Liu, C.; Cendejas, M.; Hermans, I.; Zhang, X.; Zhang, J.; Huang, J. 2D Covalent Organic Frameworks as Intrinsic Photocatalysts for Visible

Light-Driven CO₂ Reduction. *J. Am. Chem. Soc.* **2018**, *140*, 14614–14618.

(19) Zhang, J.; Han, X.; Wu, X.; Liu, Y.; Cui, Y. Multivariate Chiral Covalent Organic Frameworks with Controlled Crystallinity and Stability for Asymmetric Catalysis. *J. Am. Chem. Soc.* **2017**, *139*, 8277–8285.

(20) Ghazi, Z. A.; Zhu, L.; Wang, H.; Naeem, A.; Khattak, A. M.; Liang, B.; Khan, N. A.; Wei, Z.; Li, L.; Tang, Z. Efficient Polysulfide Chemisorption in Covalent Organic Frameworks for High-Performance Lithium-Sulfur Batteries. *Adv. Energy Mater.* **2016**, *6*, 1601250.

(21) Halder, A.; Ghosh, M.; Khayum M, A.; Bera, S.; Addicoat, M.; Sasmal, H. S.; Karak, S.; Kurungot, S.; Banerjee, R. Interlayer Hydrogen-Bonded Covalent Organic Frameworks as High-Performance Supercapacitors. *J. Am. Chem. Soc.* **2018**, *140*, 10941–10945.

(22) Lv, J.; Tan, Y.-X.; Xie, J.; Yang, R.; Yu, M.; Sun, S.; Li, M.-D.; Yuan, D.; Wang, Y. Direct Solar-to-Electrochemical Energy Storage in a Functionalized Covalent Organic Framework. *Angew. Chem., Int. Ed.* **2018**, *57*, 12716–12720.

(23) Mulzer, C. R.; Shen, L.; Bisbey, R. P.; McKone, J. R.; Zhang, N.; Abruña, H. D.; Dichtel, W. R. Superior Charge Storage and Power Density of a Conducting Polymer-Modified Covalent Organic Framework. *ACS Cent. Sci.* **2016**, *2*, 667–673.

(24) Wei, H.; Ning, J.; Cao, X.; Li, X.; Hao, L. Benzotrithiophene-Based Covalent Organic Frameworks: Construction and Structure Transformation under Ionothermal Condition. *J. Am. Chem. Soc.* **2018**, *140*, 11618–11622.

(25) Wu, X.; Han, X.; Xu, Q.; Liu, Y.; Yuan, C.; Yang, S.; Liu, Y.; Jiang, J.; Cui, Y. Chiral BINOL-Based Covalent Organic Frameworks for Enantioselective Sensing. *J. Am. Chem. Soc.* **2019**, *141*, 7081–7089.

(26) Ascherl, L.; Evans, E. W.; Hennemann, M.; Di Nuzzo, D.; Hufnagel, A. G.; Beetz, M.; Friend, R. H.; Clark, T.; Bein, T.; Auras, F. Solvatochromic Covalent Organic Frameworks. *Nat. Commun.* **2018**, *9*, 3802.

(27) Das, G.; Biswal, B. P.; Kandambeth, S.; Venkatesh, V.; Kaur, G.; Addicoat, M.; Heine, T.; Verma, S.; Banerjee, R. Chemical Sensing in Two Dimensional Porous Covalent Organic Nanosheets. *Chem. Sci.* **2015**, *6*, 3931–3939.

(28) Ding, S.-Y.; Dong, M.; Wang, Y.-W.; Chen, Y.-T.; Wang, H.-Z.; Su, C.-Y.; Wang, W. Thioether-Based Fluorescent Covalent Organic Framework for Selective Detection and Facile Removal of Mercury(II). *J. Am. Chem. Soc.* **2016**, *138*, 3031–3037.

(29) Hao, Q.; Zhao, C.; Sun, B.; Lu, C.; Liu, J.; Liu, M.; Wan, L.-J.; Wang, D. Confined Synthesis of Two-Dimensional Covalent Organic Framework Thin Films within Superspreading Water Layer. *J. Am. Chem. Soc.* **2018**, *140*, 12152–12158.

(30) Peng, Y.; Huang, Y.; Zhu, Y.; Chen, B.; Wang, L.; Lai, Z.; Zhang, Z.; Zhao, M.; Tan, C.; Yang, N.; Shao, F.; Han, Y.; Zhang, H. Ultrathin Two-Dimensional Covalent Organic Framework Nanosheets: Preparation and Application in Highly Sensitive and Selective DNA Detection. *J. Am. Chem. Soc.* **2017**, *139*, 8698–8704.

(31) Wang, P.; Zhou, F.; Zhang, C.; Yin, S.-Y.; Teng, L.; Chen, L.; Hu, X.-X.; Liu, H.-W.; Yin, X.; Zhang, X.-B. Ultrathin Two-Dimensional Covalent Organic Framework Nanoprobe for Interference-Resistant Two-Photon Fluorescence Bioimaging. *Chem. Sci.* **2018**, *9*, 8402–8408.

(32) Fang, Q.; Wang, J.; Gu, S.; Kaspar, R. B.; Zhuang, Z.; Zheng, J.; Guo, H.; Qiu, S.; Yan, Y. 3D Porous Crystalline Polyimide Covalent Organic Frameworks for Drug Delivery. *J. Am. Chem. Soc.* **2015**, *137*, 8352–8355.

(33) Mitra, S.; Sasmal, H. S.; Kundu, T.; Kandambeth, S.; Illath, K.; DíazDíaz, D.; Banerjee, R. Targeted Drug Delivery in Covalent Organic Nanosheets (CONs) via Sequential Postsynthetic Modification. *J. Am. Chem. Soc.* **2017**, *139*, 4513–4520.

(34) Vyas, V. S.; Vishwakarma, M.; Moudrakovski, I.; Haase, F.; Savasci, G.; Ochsenfeld, C.; Spatz, J. P.; Lotsch, B. V. Exploiting Noncovalent Interactions in an Imine-Based Covalent Organic Framework for Quercetin Delivery. *Adv. Mater.* **2016**, *28*, 8749–8754.

(35) Zhang, G.; Li, X.; Liao, Q.; Liu, Y.; Xi, K.; Huang, W.; Jia, X. Water-Dispersible PEG-Curcumin/Amine-Functionalized Covalent Organic Framework Nanocomposites as Smart Carriers for in Vivo Drug Delivery. *Nat. Commun.* **2018**, *9*, 2785.

(36) Bessinger, D.; Ascherl, L.; Auras, F.; Bein, T. Spectrally Switchable Photodetection with Near-Infrared-Absorbing Covalent Organic Frameworks. *J. Am. Chem. Soc.* **2017**, *139*, 12035–12042.

(37) Ding, H.; Li, J.; Xie, G.; Lin, G.; Chen, R.; Peng, Z.; Yang, C.; Wang, B.; Sun, J.; Wang, C. An AIEgen-Based 3D Covalent Organic Framework for White Light-Emitting Diodes. *Nat. Commun.* **2018**, *9*, 5234.

(38) Feng, X.; Liu, L.; Honsho, Y.; Saeki, A.; Seki, S.; Irle, S.; Dong, Y.; Nagai, A.; Jiang, D. High-Rate Charge-Carrier Transport in Porphyrin Covalent Organic Frameworks: Switching from Hole to Electron to Ambipolar Conduction. *Angew. Chem., Int. Ed.* **2012**, *51*, 2618–2622.

(39) Haldar, S.; Chakraborty, D.; Roy, B.; Banappanavar, G.; Rinku, K.; Mullangi, D.; Hazra, P.; Kabra, D.; Vaidhyanathan, R. Anthracene-Resorcinol Derived Covalent Organic Framework as Flexible White Light Emitter. *J. Am. Chem. Soc.* **2018**, *140*, 13367–13374.

(40) Medina, D. D.; Sick, T.; Bein, T. Photoactive and Conducting Covalent Organic Frameworks. *Adv. Energy Mater.* **2017**, *7*, 1700387.

(41) Spitzer, E. L.; Dichtel, W. R. Lewis Acid-Catalysed Formation of Two-Dimensional Phthalocyanine Covalent Organic Frameworks. *Nat. Chem.* **2010**, *2*, 672–677.

(42) Wan, S.; Guo, J.; Kim, J.; Ihee, H.; Jiang, D. A Belt-Shaped, Blue Luminescent, and Semiconducting Covalent Organic Framework. *Angew. Chem., Int. Ed.* **2008**, *47*, 8826–8830.

(43) Liu, W.; Su, Q.; Ju, P.; Guo, B.; Zhou, H.; Li, G.; Wu, Q. A Hydrazone-Based Covalent Organic Framework as an Efficient and Reusable Photocatalyst for the Cross-Dehydrogenative Coupling Reaction of N-Aryltetrahydroisoquinolines. *ChemSusChem* **2017**, *10*, 664–669.

(44) Zhi, Y.; Li, Z.; Feng, X.; Xia, H.; Zhang, Y.; Shi, Z.; Mu, Y.; Liu, X. Covalent Organic Frameworks as Metal-Free Heterogeneous Photocatalysts for Organic Transformations. *J. Mater. Chem. A* **2017**, *5*, 22933–22938.

(45) Chen, R.; Shi, J.-L.; Ma, Y.; Lin, G.; Lang, X.; Wang, C. Designed Synthesis of a 2D Porphyrin-Based sp² Carbon-Conjugated Covalent Organic Framework for Heterogeneous Photocatalysis. *Angew. Chem., Int. Ed.* **2019**, *58*, 6430–6434.

(46) Wei, P.-F.; Qi, M.-Z.; Wang, Z.-P.; Ding, S.-Y.; Yu, W.; Liu, Q.; Wang, L.-K.; Wang, H.-Z.; An, W.-K.; Wang, W. Benzoxazole-Linked Ultrastable Covalent Organic Frameworks for Photocatalysis. *J. Am. Chem. Soc.* **2018**, *140*, 4623–4631.

(47) (a) Liang, R.-R.; Xu, S.-Q.; Pang, Z.-F.; Qi, Q.-Y.; Zhao, X. Self-Sorted Pore-Formation in the Construction of Heteropore Covalent Organic Frameworks Based on Orthogonal Reactions. *Chem. Commun.* **2018**, *54*, 880–883.

(48) Pang, Z.-F.; Xu, S.-Q.; Zhou, T.-Y.; Liang, R.-R.; Zhan, T.-G.; Zhao, X. Construction of Covalent Organic Frameworks Bearing Three Different Kinds of Pores through the Heterostructural Mixed Linker Strategy. *J. Am. Chem. Soc.* **2016**, *138*, 4710–4713.

(49) Zeng, Y.; Zou, R.; Luo, Z.; Zhang, H.; Yao, X.; Ma, X.; Zou, R.; Zhao, Y. Covalent Organic Frameworks Formed with Two Types of Covalent Bonds Based on Orthogonal Reactions. *J. Am. Chem. Soc.* **2015**, *137*, 1020–1023.

(50) Jin, Y.; Hu, Y.; Zhang, W. Tessellated Multiporous Two-Dimensional Covalent Organic Frameworks. *Nat. Rev. Chem.* **2017**, *1*, 0056.

(51) Smith, B. J.; Dichtel, W. R. Mechanistic Studies of Two-Dimensional Covalent Organic Frameworks Rapidly Polymerized from Initially Homogenous Conditions. *J. Am. Chem. Soc.* **2014**, *136*, 8783–8789.

(52) Seo, J.-M.; Noh, H.-J.; Jeong, H. Y.; Baek, J.-B. Converting Unstable Imine-Linked Network into Stable Aromatic Benzoxazole-Linked One via Post-oxidative Cyclization. *J. Am. Chem. Soc.* **2019**, *141*, 11786–11790.

(53) Li, Y.; Chen, Q.; Xu, T.; Xie, Z.; Liu, J.; Yu, X.; Ma, S.; Qin, T.; Chen, L. De Novo Design and Facile Synthesis of 2D Covalent Organic Frameworks: A Two-in-One Strategy. *J. Am. Chem. Soc.* **2019**, *141*, 13822–13828.

(54) Gao, C.; Li, J.; Yin, S.; Lin, G.; Ma, T.; Meng, Y.; Sun, J.; Wang, C. Isostructural Three-Dimensional Covalent Organic Frameworks. *Angew. Chem., Int. Ed.* **2019**, *58*, 9770–9775.

(55) Uribe-Romo, F. J.; Hunt, J. R.; Furukawa, H.; Klöck, C.; O’Keeffe, M.; Yaghi, O. M. A Crystalline Imine-Linked 3-D Porous Covalent Organic Framework. *J. Am. Chem. Soc.* **2009**, *131*, 4570–4571.

(56) Burton, G. W.; Doba, T.; Gabe, E.; Hughes, L.; Lee, F. L.; Prasad, L.; Ingold, K. U. Autoxidation of Biological Molecules. 4. Maximizing the Antioxidant Activity of Phenols. *J. Am. Chem. Soc.* **1985**, *107*, 7053–7065.

(57) Greenberg, M.; Dodds, M.; Tian, M. Naturally Occurring Phenolic Antibacterial Compounds Show Effectiveness against Oral Bacteria by a Quantitative Structure–Activity Relationship Study. *J. Agric. Food Chem.* **2008**, *56*, 11151–11156.

(58) Quideau, S.; Deffieux, D.; Douat-Casassus, C.; Pouysegu, L. Plant Polyphenols: Chemical Properties, Biological Activities, and Synthesis. *Angew. Chem., Int. Ed.* **2011**, *50*, 586–621.

(59) Johnson, J. A.; Luo, J.; Zhang, X.; Chen, Y.-S.; Morton, M. D.; Echeverria, E.; Torres, F. E.; Zhang, J. Porphyrin-Metalation-Mediated Tuning of Photoredox Catalytic Properties in Metal–Organic Frameworks. *ACS Catal.* **2015**, *5*, 5283–5291.

(60) Pitre, S. P.; McTiernan, C. D.; Ismaili, H.; Scaiano, J. C. Mechanistic Insights and Kinetic Analysis for the Oxidative Hydroxylation of Arylboronic Acids by Visible Light Photoredox Catalysis: A Metal-Free Alternative. *J. Am. Chem. Soc.* **2013**, *135*, 13286–13289.

(61) Sun, L.; Li, R.; Zhan, W.; Yuan, Y.; Wang, X.; Han, X.; Zhao, Y. Double-Shelled Hollow Rods Assembled from Nitrogen/Sulfur-Codoped Carbon Coated Indium Oxide Nanoparticles as Excellent Photocatalysts. *Nat. Commun.* **2019**, *10*, 2270.

(62) Zou, Y.-Q.; Chen, J.-R.; Liu, X.-P.; Lu, L.-Q.; Davis, R. L.; Jørgensen, K. A.; Xiao, W.-J. Highly Efficient Aerobic Oxidative Hydroxylation of Arylboronic Acids: Photoredox Catalysis Using Visible Light. *Angew. Chem., Int. Ed.* **2012**, *51*, 784–788.